# A regulative epigenetic circuit supervised by HDAC7 represses IGFBP6 and IGFBP7 expression to sustain mammary stemness

Eros Di Giorgio‡,1 [ID], Valentina Cutano‡,1, Martina Minisini1, Vanessa Tolotto1, Emiliano Dalla1 [ID] & Claudio Brancolini*,1 [ID]

1Department of Medicine, Università degli Studi di Udine. P.le Kolbe 4, Udine, 33100, Italy
*Author for correspondence: claudio.brancolini@uniud.it
‡Authors contributed equally

**Background:** In the breast, the pleiotropic epigenetic regulator HDAC7 can influence stemness. **Materials & Methods:** The authors used MCF10 cells knocked-out for HDAC7 to explore the contribution of HDAC7 to IGF1 signaling. **Results:** HDAC7 buffers H3K27ac levels at the IGFBP6 and IGFBP7 genomic loci and influences their expression. In this manner, HDAC7 can tune IGF1 signaling to sustain stemness. In HDAC7 knocked-out cells, RXRA promotes the upregulation of IGFBP6/7 mRNAs. By contrast, HDAC7 increases FABP5 expression, possibly through repression of miR-218. High levels of FABP5 can reduce the delivery of all-trans-retinoic acid to RXRA. Accordingly, the silencing of FABP5 increases IGFBP6 and IGFBP7 expression and reduces mammosphere generation. **Conclusion:** The authors propose that HDAC7 controls the uptake of all-trans-retinoic acid, thus influencing RXRA activity and IGF1 signaling.

HDAC7 belongs to the class IIa HDAC family, which includes pleiotropic epigenetic regulators. HDAC7 plays important roles in several differentiation decisions and adaptive responses in adults [1,2]. This class IIa member is abundantly expressed in the breast, where it plays a part in the control of proliferation and in the morphogenetic process. These actions are instrumental in allowing acini formation *in vitro* [3,4].

The microenvironment plays a key role in sculpting the epigenome to maintain tissue homeostasis [5]. Its action influences different cell populations, including the pool of tissue-specific stem cells. Specifically, the microenvironment modulates the regenerative capabilities of stem cells by influencing the activity of several signaling pathways that control stem cell behavior [6].

HDAC7 can also regulate stem cell functions, particularly in the breast. Its actions are mediated at the level of both the microenvironment and intrinsic stemness program regulation [7–10]. Several secreted factors that create and sculpt the microenvironment are under the repressive action of HDAC7 [9]. The microenvironment is fundamental in supervising and maintaining breast stem cell properties. Deletion of HDAC7 unleashes the expression of negative regulators of stemness, such as IL-24, and dramatically impairs mammosphere generation [9,11].

IGF1 is an important determinant of mammary terminal end bud and ductal formation during development [12]. In addition, IGF1 plays significant roles in breast cancer development, progression and metastasis [13]. IGF1 signaling is finely tuned through a complex network of signaling molecules, which comprise IGFBPs, IGF1R and specific transducers. IGF1 is implicated in breast cancer development, and IGF1R signaling contributes to breast cancer stem cell maintenance [14,15]. *IGFBP6* and *IGFBP7* are among the genes regulated by HDAC7 in breast cells [9]. However, how HDAC7 can regulate their expression and whether epigenetic status at the *IGFBP6* and *IGFBP7* loci is modulated by HDAC7 are currently unknown. For these reasons, the authors, in this study, investigated additional mechanisms engaged by HDAC7 in the maintenance of stemness in MCF10A mammary epithelial cells. The authors dissected the regulation driven by HDAC7 to control the expression of *IGFBP6* and *IGFBP7*, two additional putative anti-stem factors capable of influencing IGF1 signaling.

Future Medicine

## Methods

### Cell cultures & reagents

MCF10A cells were grown as previously described [4]. HEK293T and AMPHO cells were grown in Dulbecco's modified Eagle medium (DMEM) supplemented with 10% fetal bovine serum. MCF10A/$HDAC7^{-/-}$ cells and the same cells expressing the inducible form of HDAC7 were grown in complete F12/DMEM medium without phenol red (Sigma-Aldrich, MO, USA) and with 5% charcoal-stripped horse serum [9], and 4-OHT (Sigma-Aldrich) was used at 1 μM. In all media, L-glutamine (2 mM), penicillin (100 U/ml) and streptomycin (100 μg/ml) (Euroclone, Milan, Italy) were added.

### Mammosphere assays

Mammospheres were grown in mammosphere medium composed of Ham's F12/DMEM 1:1 medium (Sigma-Aldrich) supplemented with B27 (1x, Gibco, MA, USA) and EGF (20 ng/ml, PeproTech, London, UK). Next, $1 \times 10^3$ trypan blue-negative cells were seeded in ultra low-attachment multiwells (Corning, NY, USA) and cultivated for 10 days. For IGF1 (20 ng/ml) (PeproTech) treatments, MCF10A cells were pre-treated for 2 days. For the evaluation of *FABP5* silencing and miR-21 and miR-218 mimicking effects on mammosphere formation, interfering RNAs were delivered using Lipofectamine 2000 (ThermoFisher, MA, USA). After 24 h, cells were harvested and cultured for 5 days in ultra low-attachment plates. The efficiency of the interference was evaluated using parallel cultures after 72 h of silencing. Images were collected with a Leica AF 6000LX microscope (Leica Microsystems, Mannheim, Germany). Spheres over 50 μm in diameter were counted. Area was measured with ImageJ software as previously described [16].

### Immunofluorescence, immunoprecipitation & immunoblotting

After transfection, HEK293 cells were fixed with 3% paraformaldehyde and permeabilized with 0.1% Triton X-100 (Sigma-Aldrich). Immunofluorescence was performed using anti-FLAG M2 antibody. The secondary antibodies were Alexa Fluor 546-conjugated goat anti-mouse antibodies (A-11030; Thermo Fisher Scientific). Cells were imaged with a Leica confocal scanner SP2 microscope equipped with a 488-λ argon laser and a 543–633-λ helium–neon laser. For co-immunoprecipitation, cells were lysed in a hypotonic buffer (20 mM Tris-HCl, pH 7.5; 10 mM MgCl2; 10 mM KCl; and 1% Triton X-100) supplemented with protease and phosphatase inhibitors. For each immunoprecipitation, 1 μg of anti-HDAC7 or anti-GFP antibodies was used. Protein complexes were collected with Protein A Sepharose beads and processed for SDS-page (Merck KGaA, Darmstadt, Germany) [17]. For immunoblotting, cell lysates after SDS-PAGE and immunoblotting were incubated with primary antibodies as previously described [17]. Secondary antibodies were obtained from Sigma-Aldrich (peroxidase-conjugated goat anti-rabbit IgG A05451 and peroxidase-conjugated goat anti-mouse IgG A4416), and blots were developed with SuperSignal west dura (Pierce, MA, USA).

### Antibodies

The primary antibodies used were against MEF2D (610774; BD Biosciences, CA, USA), actin (A2066; Sigma-Aldrich), FLAG M2 (F1804; Sigma-Aldrich), GFP and HDAC4 [18], HDAC7 [9], RXR alpha (D-20; Santa Cruz Biotechnology, TX, USA), H3K27ac (ab4729; Abcam, MA, USA), CRABP2 (sc-166897; Santa-Cruz Biotechnology) and FABP5 (sc-365236; Santa-Cruz Biotechnology).

### Plasmid transfection, siRNA delivery & luciferase assay on FABP5 3′UTR

The generation of the pEGFP-N1-MEF2D plasmid was previously described [17]. The CDS of RXRA (NM_002957) and CDS of USP33 (NM_015017) were cloned in pEGFP N1 using a PCR/restriction-based method (RXRA forward [FW]: AAAGAATTCCTAAGTCATTTGGTGCGG, reverse [RV]: AAAAGATCTATG-GACACCAAACATTTCC; USP33 FW: GGCGGATCCATGACAGGATCAAATTCACAC, RV: AAAGGATC-CAACAAAGACCGAGTTTCTACTTGAA), and pFLAG CMV5a HDAC7 was obtained by subcloning the CDS of HDAC7 (NM_015401) from pWZL HDAC7 GFP [19]. The 205-bp-long 3′UTR of FABP5 was cloned in pGL3 control by means of a PCR/restriction-based method using 50 ng of gDNA extracted from MCF10A cells as a template and primers bearing the restriction sites of XbaI (FW: AAATCTAGAGTAAATTCCATCATCACTTTGG, RV: AAATCTAGAAGCACAAACACATTTATTTATTA).

For silencing and delivery of miRNA mimics, 74 pmol of siRNA duplex against RXRA (GGGA-GAAGGUCUAUGCGUC), FOXA1 (CCAUGAACACCUACAUGACCAUG), FABP5 (GUGCAUUGGU-

UCAGCAUCA), miR-21 (HMI0371) and miR-218 (HMI0384) was delivered to MCF10A cells using Lipofectamine 2000 as a transfection reagent. Equal amounts of scramble control siRNA ware used as a control (UAAGGCUAUGAAGAGAUAC; Sigma-Aldrich).

For luciferase assay, 1 μg of pGL3 control or pGL3 control 3′UTR FABP5 and 100 ng of pRenilla were transfected in MCF10A *HDAC7*^{+/+} and *HDAC7*^{−/−} cells. After 48 h, cells were lysed and processed using the Dual-Luciferase reporter assay system (Promega, WI, USA).

### RNA extraction & quantitative real-time PCR

Cells were lysed using TRI Reagent (Molecular Research Center, OH, USA). Next, 1.0 μg of total RNA was retrotranscribed using 100 units of M-MLV reverse transcriptase (Life Technologies, MA USA). Quantitative real-time PCR (qRT-PCR) was performed using SYBR green technology (Kapa Biosystems, MA, USA). Data were analyzed by comparative threshold cycle using HPRT and GAPDH as normalizers.

### RNA expression array & data analysis

RNA expression experiments were performed as previously described [9]. Fold change and p-values for each probe set were calculated using a moderated t-statistic in the limma package [20], with the variance estimate being adjusted by incorporating global variation measures for the complete set of probes on the array. All p-values were then corrected for multiple hypothesis testing using the Benjamini–Hochberg method. Differentially expressed genes were selected based on fold changes and adjusted $p < 0.05$.

### Chromatin immunoprecipitation, library construction, chromatin immunoprecipitation sequencing & next-generation sequencing data analysis

For chromatin immunoprecipitation sequencing (ChIP-seq) experiments, 50 μg of chromatin was immunoprecipitated using 2 μg of anti-H3K27ac (ab4729; Abcam) or 6 μg of anti-HDAC7 antibody or control IgG. After RNAseA treatment (Ambion, MA, USA) and de-crosslinking, DNA was purified with Zymo ChIP columns. Next, 5 ng of total DNA obtained by pulling three independent experiments was used to prepare ChIP-seq libraries according to the TruSeq ChIP sample preparation guide (Illumina, CA, USA). Libraries were sequenced on the Illumina HiSeq 2000 sequencer. Sequencing reads from ChIP-seq experiments were aligned to the National Center for Biotechnology Information GRCh38 human reference with Bowtie 2 [21]. Peak heat maps, gene annotation and the resulting Venn diagrams and bar plots representing peak localization in genomic elements/distance from the transcription start site (TSS) were obtained using the ChIPseeker and Gviz R/Bioconductor packages [22–24]. Quantitative PCR was used to validate ChIP-seq data on the *IGFBP6* and *IGFBP7* loci using the primers *IGFBP6* TSS FW: TCCAGTCCCACCCAGTTTAG, RV: GGTCATGGTCAGGGTTTGTG; *IGFBP7* INTRON1 FW: AGCCAGGATTCAGGGTAGGT, RV: GAGACCCTGTGTTGGGCTAA; and *IGFBP7* TSS FW: CTTTACC-CTTCCGCCTCTTG, RV: CTCTTCCTCCTCTTCGGACA.

### *In silico* miRNA target analysis

The authors queried the TarBase v8 database (https://carolina.imis.athena-innovation.gr/diana_tools/web/index.php?r=tarbasev8%2Findex) to identify miRNAs that were validated as regulators of the *FABP5* gene. The authors queried five databases of miRNA predicted targets, miRWalk (http://mirwalk.umm.uni-heidelberg.de/), TargetScan (www.targetscan.org/vert_72/), miRDB (http://mirdb.org/cgi-bin/search.cgi), miRSystem (http://mirsystem.cgm.ntu.edu.tw/index.php) and miRmap (https://mirmap.ezlab.org/app/), retaining the results confirmed by at least four different approaches.

### Detection of miRNA expression

For quantification of mature miRNA, stem–loop RT-PCR was performed in a manner similar to that used by Chen *et al.* [25]. The first reverse transcription was performed using 0.25 μM specific primers (Table 1) and 1 μM random hexamers (Promega). For quantitative PCR, a specific FW primer and a universal RV primer complementary to the stem–loop were used. Normalization was performed with respect to U6.

| Table 1. Oligonucleotides used to analyze miRNA expression. | |
| --- | --- |
| Oligo name | Sequence 5′ to 3′ |
| Common RV PCR | GTGCAGGGTCCGAGGT |
| hsa-miR-144-5p RT | GTCGTATCCAGTGCAGGGTCCGAGGTATTCGCACTGGATACGACTTACA |
| hsa-miR-144-3p RT | GTCGTATCCAGTGCAGGGTCCGAGGTATTCGCACTGGATACGAAGTACA |
| hsa-miR-144-5p PCR | GGATATCATCATATAC |
| hsa-miR-144-3p PCR | UACAGTATAGATGATG |
| hsa-miR-20a-5p RT | GTCGTATCCAGTGCAGGGTCCGAGGTATTCGCACTGGATACGA |
| hsa-miR-20a-3p RT | GTCGTATCCAGTGCAGGGTCCGAGGTATTCGCACTGGCTTTAA |
| hsa-miR-20a-5p PCR | TAAAGTGCTTATAGTG |
| hsa-miR-20a-3p PCR | ACTGCATTATGAGCAC |
| hsa-miR-21-5p RT | GTCGTATCCAGTGCAGGGTCCGAGGTATTCGCACTGGATACGATCAACT |
| hsa-miR-21-3p RT | GTCGTATCCAGTGCAGGGTCCGAGGTATTCGCACTGGATACGATGTGCC |
| hsa-miR-21-5p PCR | TAGCTTATCAGACTGA |
| hsa-miR-21-3p PCR | CAACACCAGTCGATGG |
| hsa-miR-218-5p RT | GTCGTATCCAGTGCAGGGTCCGAGGTATTCGCACTGGATACGAACATGG |
| hsa-miR-218-3p RT | GTCGTATCCAGTGCAGGGTCCGAGGTATTCGCACTGGATACGACCATGG |
| hsa-miR-218-5p PCR | UTGTGCTTGATCTAAC |
| hsa-miR-218-3p PCR | ATGGTTCCGTCAAGCA |
| hsa-miR-202-5p RT | GTCGTATCCAGTGCAGGGTCCGAGGTATTCGCACTGGATACGACAAAGA |
| hsa-miR-202-3p RT | GTCGTATCCAGTGCAGGGTCCGAGGTATTCGCACTGGATACGATTCCCA |
| hsa-miR-202-5p PCR | TTCCTATGCATATACT |
| hsa-miR-202-3p PCR | AGAGGTATAGGGCATG |
| IGFBP7 FW | GCTCAAGTACACCTGGGCAC |
| IGFBP7 RV | CATCACCCAGGTCAGCAAG |
| IGFBP6 FW | ATCCGCCCAAGGACGAC |
| IGFBP6 RV | GCCTGCTTGGGGTTTACTCT |
| HPRT FW | AGACTTTGCTTTCCTTGGTCAGG |
| HPRT RV | GTCTGGCTTATATCCAACACTTCG |
| FOXA1 FW | CTGTGAAGATGGAAGGGCAT |
| FOXA1 RV | GCCTGAGTTCATGTTGCTGA |
| RXRA FW | GAGTGTACAGCTGCGAGGG |
| RXRA RV | TGTCAATCAGGCAGTTCCTTG |
| U6 FW | AAACCTGGCTGCGGTTGGCATGGAC |
| U6 RV | CACCGTCCATGCCAACCGCAGCCAG |
| FW: Forward; RT: Reverse transcription; RV: Reverse. | |

## Statistical analysis

The Student's t-test was used for the experimental data. Dunn's multiple comparison test was applied in case of multiple sampling. A p = 0.05 was chosen for the significance limit. Data in the figures are arithmetic means and standard deviations from at least three independent biological experiments.

## Results

### HDAC7 influences the expression of elements of IGF1 signaling

Gene expression profile studies in human mammary gland epithelial MCF10A cells knocked out for HDAC7 have revealed that some components of the IGF signaling pathway are under the regulation of this deacetylase [9]. The authors decided to analyze in a comprehensive manner the mRNA levels of different elements regulating IGF1 signaling in $HDAC7^{-/-}$ and $HDAC7^{+/+}$ cells. The authors validated the results using an inducible system of HDAC7 recovery, represented by $HDAC7^{-/-}$ cells expressing HDAC7-ER fusion. As a control, $HDAC7^{-/-}$ cells expressing ER alone were used. *IGFBP6, IGFBP7, IGFL1* and *IRS2* are the genes of the IGF signaling network whose mRNA levels are significantly upregulated in the absence of HDAC7. By contrast, *IGFL2* is significantly repressed after the knockout of HDAC7, and this repression is attenuated upon reintroduction of HDAC7 (Figure 1A). The
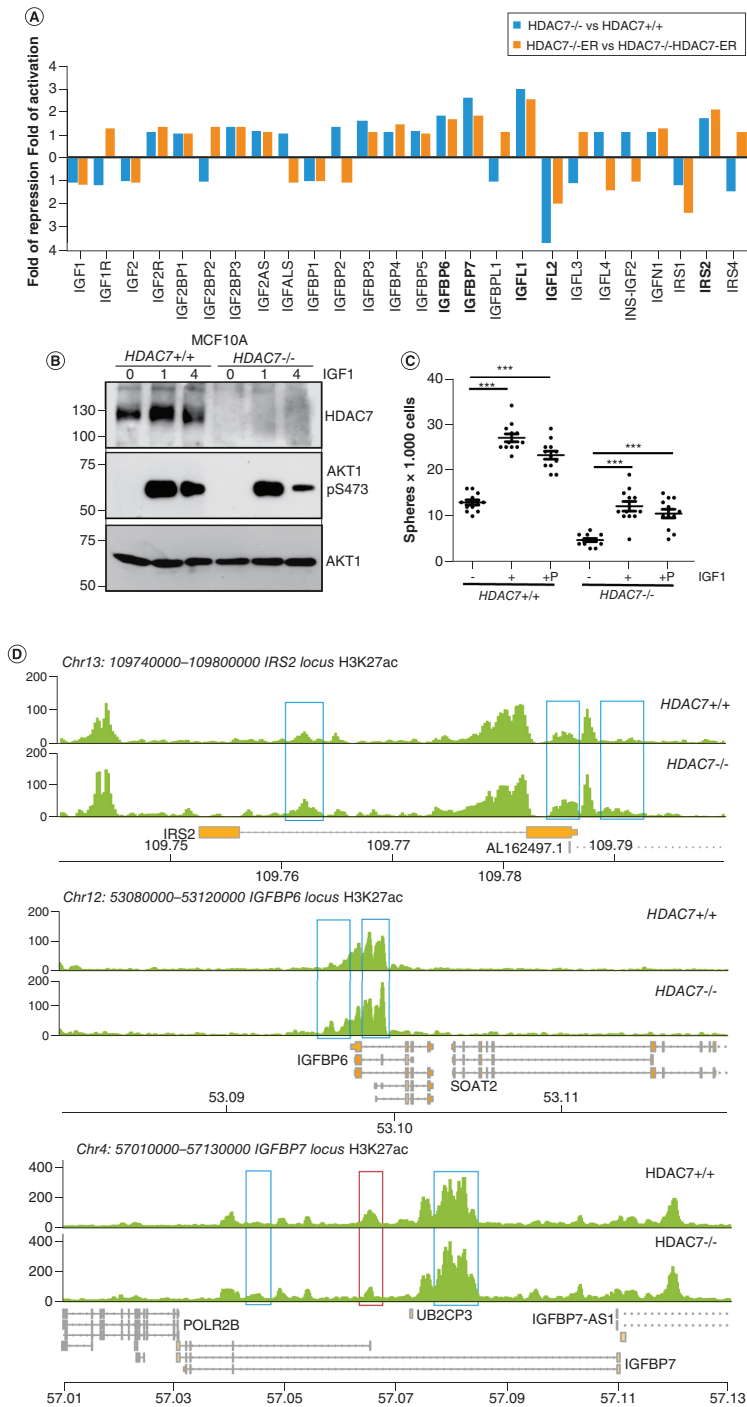
**Figure 1. IGF1 signaling under HDAC7 regulation and its impact on mammosphere generation. (A)** Histograms illustrating fold changes in the expression levels of the different elements of the IGF pathway between the different engineered MCF10A cells as indicated. **(B)** Immunoblot analysis of AKT phosphorylation in $HDAC7^{+/+}$ and $HDAC7^{-/-}$ MCF10A cells treated with IGF1. Cells were starved for 24 h and then treated for the indicated hours with IGF1 (20 ng/ml). Cellular lysates were generated and immunoblots were performed with the indicated antibodies. **(C)** Scatter dot plot illustrating the number of mammospheres generated by $HDAC7^{+/+}$ and $HDAC7^{-/-}$ MCF10A cells. In the case of IGF1, cells were pretreated for 2 days with 15 ng/ml of IGF1 or pretreated and next maintained in a medium containing IGF1 (+P). **(D)** Detailed view of H3K27ac tracks at the *IRS2*, *IGFBP6* and *IGFBP7* loci in $HDAC7^{-/-}$ and $HDAC7^{+/+}$ MCF10A cells. Gene structure and chromosomal location are shown, with the blue box highlighting differences in the enriched peaks between the two cell lines. *p < 0.05; **p < 0.01; ***p < 0.005.
Chr: Chromosome; ER: Endoplasmic reticulum.

original data are shown in Supplementary Table 1.

In MCF10A cells, and in breast cancer cells in general, HDAC7 influences multiple aspects of the transformation process, including stemness efficiency. These actions are mediated at the level of the microenvironment and by controlling intrinsic stemness programs [8–10]. Hence, the authors next investigated whether the influence of HDAC7 on IGF1 signaling may be responsible for the stemness properties of MCF10A cells. When MCF10A cells are grown in suspension, they can form spheres with low efficiency. This assay is commonly used to measure the presence of stem-like cells [9]. In the absence of HDAC7, IGF signaling could be dampened by the increased levels of IGFBP6 and IGFBP7 [26,27], and this inhibition could impact on mammosphere generation. In fact, IGF1 signaling in MCF10A cells, as measured by levels of AKT phosphorylation, is reduced in the absence of HDAC7 (Figure 1B). Accordingly, deletion of HDAC7 impairs mammosphere generation, and treatment with IGF1 potentiates sphere formation in both $HDAC7^{+/+}$ and $HDAC7^{-/-}$ cells (Figure 1C). However, even in the presence of IGF1, $HDAC7^{-/-}$ cells exhibit a deficit in sphere formation that cannot be completely reversed by the addition of IGF1. This deficit strongly suggests that HDAC7 can modulate additional intrinsic stemness programs.

Since the role of $IGFL1$ and $IGFL2$ is poorly defined in the context of IGF-signaling, the authors focused the subsequent analysis on $IGFBP6$, $IGFBP7$ and $IRS2$. The authors investigated the status of histone H3 lysine 27 acetylation (H3K27ac) by re-analyzing ChIP-seq experiments recently performed on $HDAC7^{-/-}$ and $HDAC7^{+/+}$ MCF10A cells. All three genes contain regions highly acetylated on H3K27, indicative of an open chromatin status and active transcription (Figure 1D). In general, H3K27ac signals are increased in $HDAC7^{-/-}$ cells, although with a different behavior. In the case of the $IRS2$ locus, there is an increase in H3K27ac peaks in the promoter region close to the TSS and in the 3′ end of the first intron. $IGFBP6$ shows high levels of H3K27ac around the first exon and in the first intron. In the absence of HDAC7, there is a slight increase in H3K27ac peaks. Finally, $IGFBP7$ shows a region highly enriched for H3K27ac within the first intron. In addition, there are less intense H3K27ac peaks distributed throughout its length. Ablation of HDAC7 provokes an increase in H3K37ac peaks in the highly acetylated region as well as in the less intensely acetylated regions. Curiously, a reduction in acetylation levels is also observed in a small region, as highlighted by the red box.

Upregulation of H3K27ac levels at regulatory regions of $IGFBP6/7$ loci was confirmed by quantitative ChIP-PCR analysis (Supplementary Figure 1A). By contrast, $IGFL1$ and $IGFL2$ loci were characterized by very low levels of H3K27ac, and removal of HDAC7 did not modify this profile (Supplementary Figure 1B & C).

In summary, $IGFBP6$, $IGFBP7$ and $IRS2$ loci were characterized by the presence of an open chromatin marker, indicative of active transcription. The presence of highly acetylated regions within these loci, even in $HDAC7$-expressing cells, and the moderate increases observed in HDAC7 null cells indicated that this class IIa HDAC was involved in buffering rather than switching off H3K27ac levels in these regions.

## Identification of transcription factors involved in mediating the repressive influence of HDAC7 on IGFBP6 & IGFBP7

The MEF2 family of transcription factors (TFs) are well-established partners of class IIa HDACs [2,28]. However, the upregulation of $IGFBP6$ and $IGFBP7$ seems to be independent of MEF2 transcriptional activity [9]. To identify new TFs that, under the influence of HDAC7, could regulate $IGFBP6$ and $IGFBP7$ transcription, the promoters (±5 kb from TSS) of $IGFBP6$ and $IGFBP7$ were analyzed using the LASAGNA-Search and MEME-ChIP tools [29,30]. For four TFs (FOXA1, E2F6, JUN/FOS and RUNX1), the authors also identified ChIP-seq peaks in the GTRD database (Figure 2A) [31]. When the analysis was extended to the first intron of both genes, ChIP-seq peaks corresponding to PPARG, RXRA and TFAP2A were also found. The authors focused attention on RXRA and FOXA1 since their binding sites tend to co-localize and could be involved in the co-regulation of $IGFBP6$ and $IGFBP7$ expression (Figure 2B).

To prove the contribution of FOXA1 and RXRA, the authors silenced their expression by RNAi. In $HDAC7^{+/+}$ cells, the mRNA levels of both IGFBPs were reduced after downregulation of $FOXA1$, whereas RXRA influenced only $IGFBP6$ levels. Curiously, $RXRA$ mRNA was augmented in FOXA1-silenced cells (Figure 2C). A different result was observed in $HDAC7^{-/-}$ cells. FOXA1 was necessary for $IGFBP6$ upregulation but dispensable for $IGFBP7$ upregulation. By contrast, RXRA was required for the upregulation of both IGFPBs. The efficiency of RXRA silencing was also verified at the protein level (Supplementary Figure 2A).

In summary, RXRA seemed to be responsible for the upregulation of $IGFBP6$ and $IGFBP7$ expression after the deletion of HDAC7. It is important to note that the binding sites for RXRA were relatively distant from regions subject to variation in H3K27ac context. To clarify this point, the authors explored the possibility that RXRA might
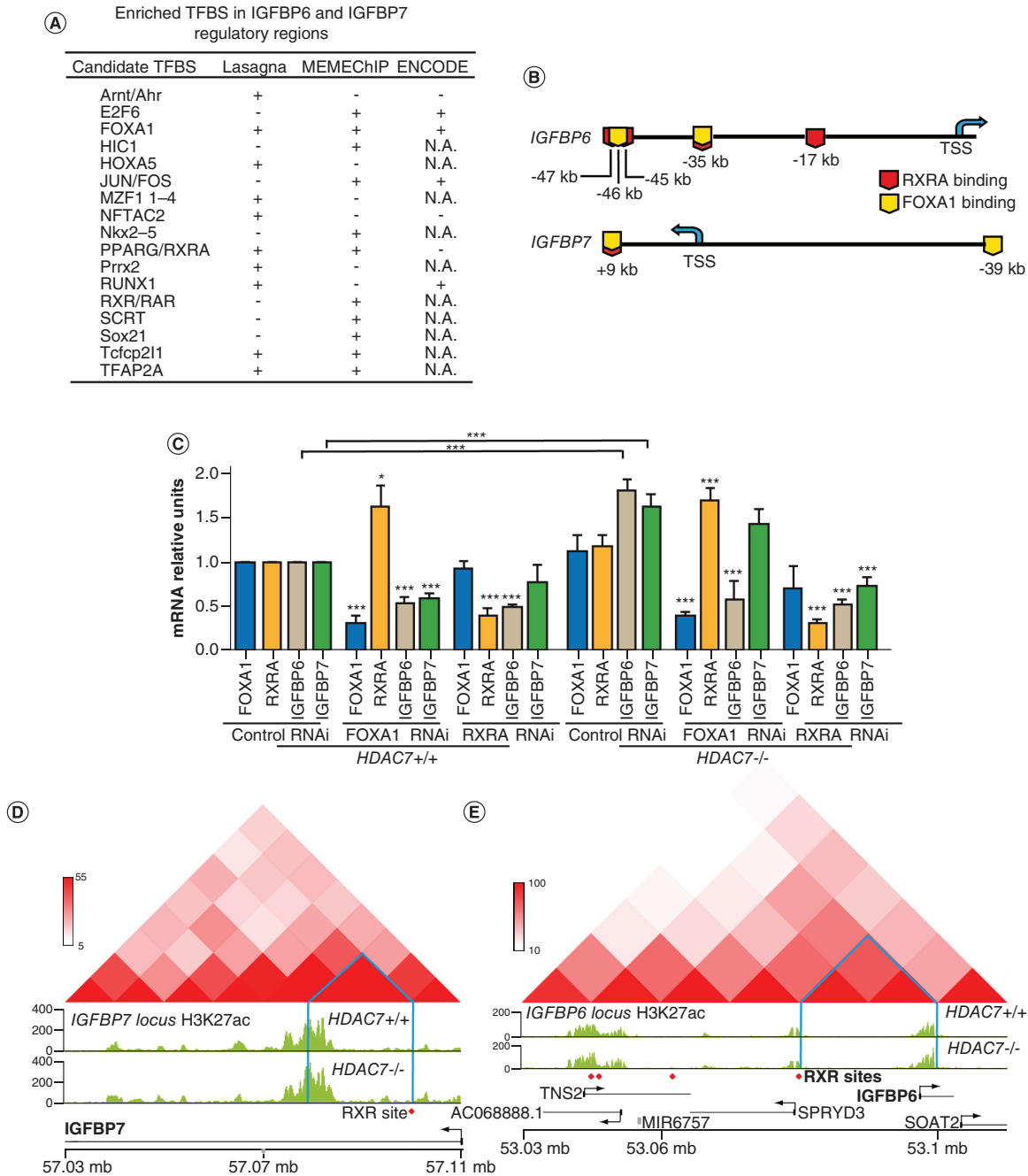
**Figure 2. RXRA regulates *IGFBP6* and *IGFBP7* mRNA levels in *HDAC7*⁻/⁻ MCF10A cells. (A)** To evaluate the existence of new transcription factors regulating *IGFBP6* and *IGFBP7* expression, the authors identified the predicted (LASAGNA and MEME-ChIP) and biologically validated (GTRD) TFBSs located in the promoters (±5 kb from the TSS) and first introns of *IGFBP6* and *IGFBP7*. TFBSs were listed alphabetically by candidate TFBS name. ChIP-seq data allowed confirmation of the binding of four transcription factors out of 17 predicted by at least one of the two bioinformatics approaches. **(B)** Schematic representation of the *IGFBP6* and *IGFBP7* loci up to 48 kb away from the TSS. Putative RXRA and FOXA1 binding sites are indicated according to GTRD data. **(C)** *HDAC7*⁺/⁺ and *HDAC7*⁻/⁻ MCF10A cells were transfected with siRNAs against RXRA or FOXA1, and after cell lysis, mRNA was extracted. The mRNA expression levels of the indicated genes were measured by quantitative real-time PCR and indicated as mean ± SD (n = 3). Significance was calculated with respect to the relative control RNAi-transfected cells unless indicated by the grafts. **(D)** RXRA/FOXA1 binding sites and H3K27ac normalized tracks are shown for WT and *HDAC7*⁻/⁻ MCF10A cells at the *IGFBP7* locus. Light blue lines evidence the chromatin looping between the RXRA site and the regulative region characterized by variation in H3K27ac levels. **(E)** RXRA/FOXA1 binding sites and H3K27ac normalized tracks are shown for wild-type and *HDAC7*⁻/⁻ MCF10A cells at the *IGFBP6* locus. Light blue lines evidence the chromatin looping between the RXRA sites and the regulative region characterized by variation in H3K27ac levels. Hi-C data [32] were used to represent the topologically associated domains within the *IGFBP6* locus (http://promoter.bx.psu.edu/hi-c/view.php).
$*p < 0.05$; $**p < 0.01$; $***p < 0.005$.
SD: Standard deviation; TFBS: Transcription factor binding site; TSS: Transcription start site.
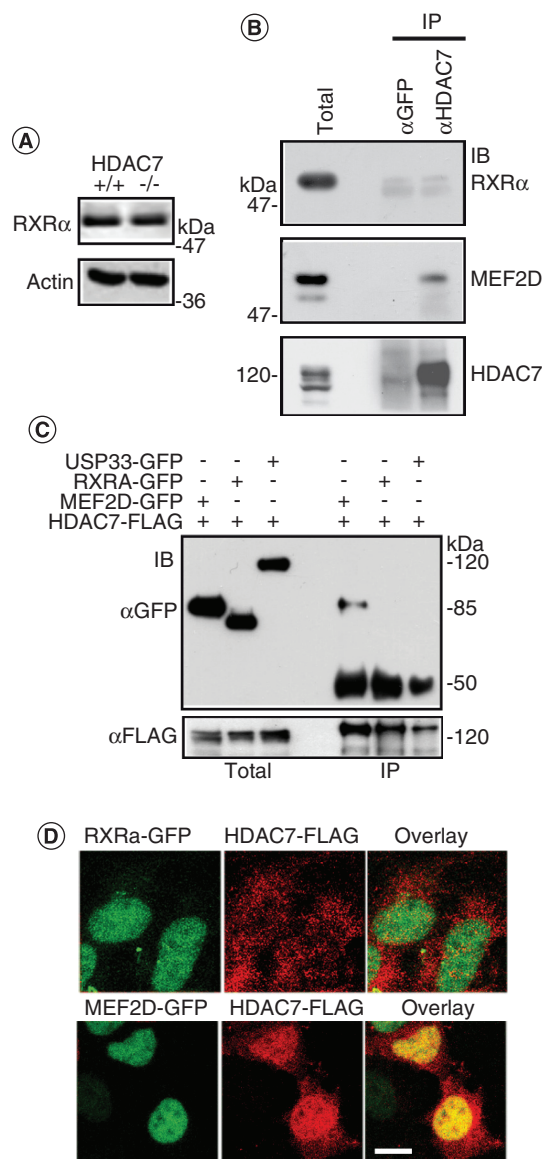
**Figure 3.    HDAC7 does not bind to RXRA. (A)** Immunoblot analysis of RXRA levels in *HDAC7*$^{-/-}$ compared with *HDAC7*$^{+/+}$ MCF10A cells. Actin was used as loading control. **(B)** Extracts from MCF10A cells were immunoprecipitated with 1 μg of anti-HDAC7 or anti-GFP antibodies as control. Next, immunocomplexes were subjected to immunoblot with the indicated antibodies. A total of 1/100 inputs have been included. **(C)** HEK293 cells were transfected with 3 μg of pFLAG-HDAC7 and 1.5 μg of pEGFP encoding for MEF2D, RXRA or USP33 as control. After 48 h, FLAG fusions were immunoprecipitated with 1 μg anti-FLAG antibody and subjected to immunoblotting with the anti-GFP antibody. After stripping, the filter was probed with anti-FLAG antibody. A total of 1/100 inputs have been included. **(D)** Immunofluorescence analysis of HEK293 cells transiently expressing the indicated transgenes. Confocal images are shown in pseudocolors. Scale bar = 50 μM.
\*p < 0.05; \*\*p < 0.01; \*\*\*p < 0.005.
IP: Immunoprecipitation.

influence H3K27ac levels at *IGFBP6/7* loci through chromosome looping. Hi-C data from MCF10A cells [32] were used to visualize the topologically associated domains as organized at the *IGFBP6/7* loci. Hi-C data indicated that the distal binding sites for RXRA lay within defined topologically associated domains, and thus a distal influence on H3K27ac levels at the *IGFBP6/7* loci by chromatin looping was possible (Figure 2D & E).

Finally, the authors also found that, similar to the two IGFBPs, upregulation of IRS2 in *HDAC7*$^{-/-}$ cells was dependent on RXRA (Supplementary Figure 2B). In this case, analysis of ChIP-seq peaks in the GTRD database revealed the binding of RXRA at the H3K27ac regulative regions of *IRS2* (Supplementary Figure 2C). Overall, similar to *IGFBP6* and *IGFBP7*, IRS2 upregulation was under the control of RXRA.

## RXRA does not bind HDAC7 & does not influence its nuclear import

HDAC7 could regulate RXRA activity through several mechanisms, including regulation of *RXRA* expression or the possibility of direct binding to the TF to repress its transcriptional activity. To understand how HDAC7 could affect RXRA activity, the authors first evaluated RXRA levels in WT and knockout cells (Figure 3A). Immunoblot confirmed the qRT-PCR data in Figure 2C, thus excluding upregulation of this TF in *HDAC7*$^{-/-}$ cells. Next, the authors evaluated whether HDAC7 and RXRA could form a complex that could explain the repressive influence of HDAC7 on *IGFBP6* and *IGFBP7* transcription. Co-immunoprecipitation experiments demonstrated that

RXRA and HDAC7 did not interact in MCF10A cells. By contrast, and as expected [33], complexes between HDAC7 and MEF2D were detected (Figure 3B). The absence of interaction was confirmed in HEK293 cells after overexpression of *HDAC7* and *RXRA* (Figure 3C). Finally, immunofluorescence analysis also evidenced a profound difference between MEF2D and RXRA in the ability to interact with HDAC7. In fact, only the co-expression of MEF2D promoted the nuclear accumulation of HDAC7 (Figure 3D).

## HDAC7 indirectly controls RXRA activity

The authors reasoned that HDAC7 could indirectly affect RXRA transcriptional activity. RXRA is a partner of different TFs via heterodimerization [34]. Moreover, retinoic acids undergo a dedicated cytosol/nuclear transport and specific metabolism [35]. To find alternative mechanisms that could explain the repressive influence of HDAC7 on RXRA, the authors compared the expression levels of several RXRA partners and several genes controlling retinoid transport/metabolism between *HDAC7*$^{+/+}$ and *HDAC7*$^{-/-}$ cells (Figure 4A). Only the expression of *FABP5*, *CRABP2* and the pseudogene *FABP5L2*, with unknown functions, was significantly downregulated in MCF10A/*HDAC7*$^{-/-}$ cells, and expression returned after HDAC7 restoration. *FABP5* and *CRABP2* encode for two high-affinity all-trans-retinoic acid (atRA) binding proteins [35]. The downregulation of *FABP5* and *CRABP2* was confirmed by qRT-PCR (Figure 4B) and immunoblot (Figure 4D). Importantly, whereas *FABP5* expression was dramatically repressed, the expression of *CRABP2* was only modestly affected. As a consequence, the ratio between the mRNAs of the two atRA binding proteins was profoundly modified by the absence of HDAC7, and this change could influence RXRA activity (Figure 4C). *FABP5* was also downregulated at the protein level in the absence of HDAC7 and upregulated after HDAC7 re-expression (Figure 4D).

To further support the role of the HDAC7/FABP5/RXRA/IGFBP circuit in mammosphere formation, the authors silenced *FABP5* expression in both *HDAC7*$^{-/-}$ and *HDAC7*$^{+/+}$ cells to assess the level of *IGFBP6/7* mRNAs (Figure 4E & F). Downregulation of *FABP5* mRNA triggered the upregulation of *IGFBP6/7* expression (Figure 4E), confirming the hypothesized circuit. Importantly, sphere generation was reduced in both *HDAC7*$^{-/-}$ and *HDAC7*$^{+/+}$ cells. The number of mammospheres was reduced (Figure 4H), as was their size (Figure 4I), thus indicating the role of FABP5 in regulating division and survival in MCF10A cells.

## HDAC7 regulates the expression of miRNAs that could control FABP5 levels

The dramatic downregulation of *FABP5* mRNA in cells null for HDAC7 suggested that this deacetylase was necessary to sustain *FABP5* transcription. To confirm this hypothesis, the authors compared the levels of H3K27ac between WT and knockout cells at the *FABP5* locus (Figure 4D). The *FABP5* locus showed a certain level of H3K27ac symptomatic of an actively transcribed gene. However, a reduction in the acetylation status was not observed in the absence of HDAC7.

An alternative hypothesis to explain the HDAC7-dependent downregulation of *FABP5* mRNA could be the existence of specific miRNAs regulated by HDAC7 and able to target *FABP5*. As a first step in validating this hypothesis, the authors isolated the 3′ untranslated region of *FABP5* and compared its stability in *HDAC7*$^{-/-}$ and *HDAC7*$^{+/+}$ cells. A Dual-Luciferase assay showed that the 3′UTR of *FABP5* was much less stable in cells deleted for HDAC7 (Figure 5B), supporting the existence of specific miRNAs, regulated by HDAC7, that target *FABP5*. Next, the authors used an *in silico* approach to identify miRNAs validated or predicted to target FABP5. After this first selection, to isolate miRNAs regulated by HDAC7, the loci containing these miRNAs were evaluated for increased levels of H3K27ac in cells knocked out of HDAC7. Finally, to understand which of the different miRNAs were directly regulated by HDAC7, the authors also evaluated the different loci for the presence of HDAC7 peaks using the ChIP-seq data. After these filtering steps, only hsa-miR-21 met all requisites, whereas hsa-miR-218 showed some HDAC7 binding, but H3K27ac levels were very low and remained unperturbed after HDAC7 deletion (Figure 5C). As controls, the authors included two miRNAs predicted to target *FABP5* (hsa-miR-144 and hsa-miR-202), but without evidence of HDAC7 binding, as well as increased H3K27ac levels in an HDAC7-dependent manner. Subsequently, the authors evaluated whether the expression levels of these miRNAs were effectively regulated by HDAC7. Figure 5D shows that, as expected from the *in silico* analysis, hsa-miR-21 expression was repressed by HDAC7. Surprisingly, despite the fact that HDAC7 did not influence H3K27ac levels at the hsa-miR-218 locus, its expression was clearly increased in MCF10A/*HDAC7*$^{-/-}$ cells. Next, the authors examined whether hsa-miR-21 and hsa-miR-218 affected *FABP5* mRNA levels. Only transfection of the hsa-miR-218 mimic was able to reduce *FABP5* expression to some extent (Figure 5E). In the mammosphere assay, hsa-miR-218 dramatically reduced the
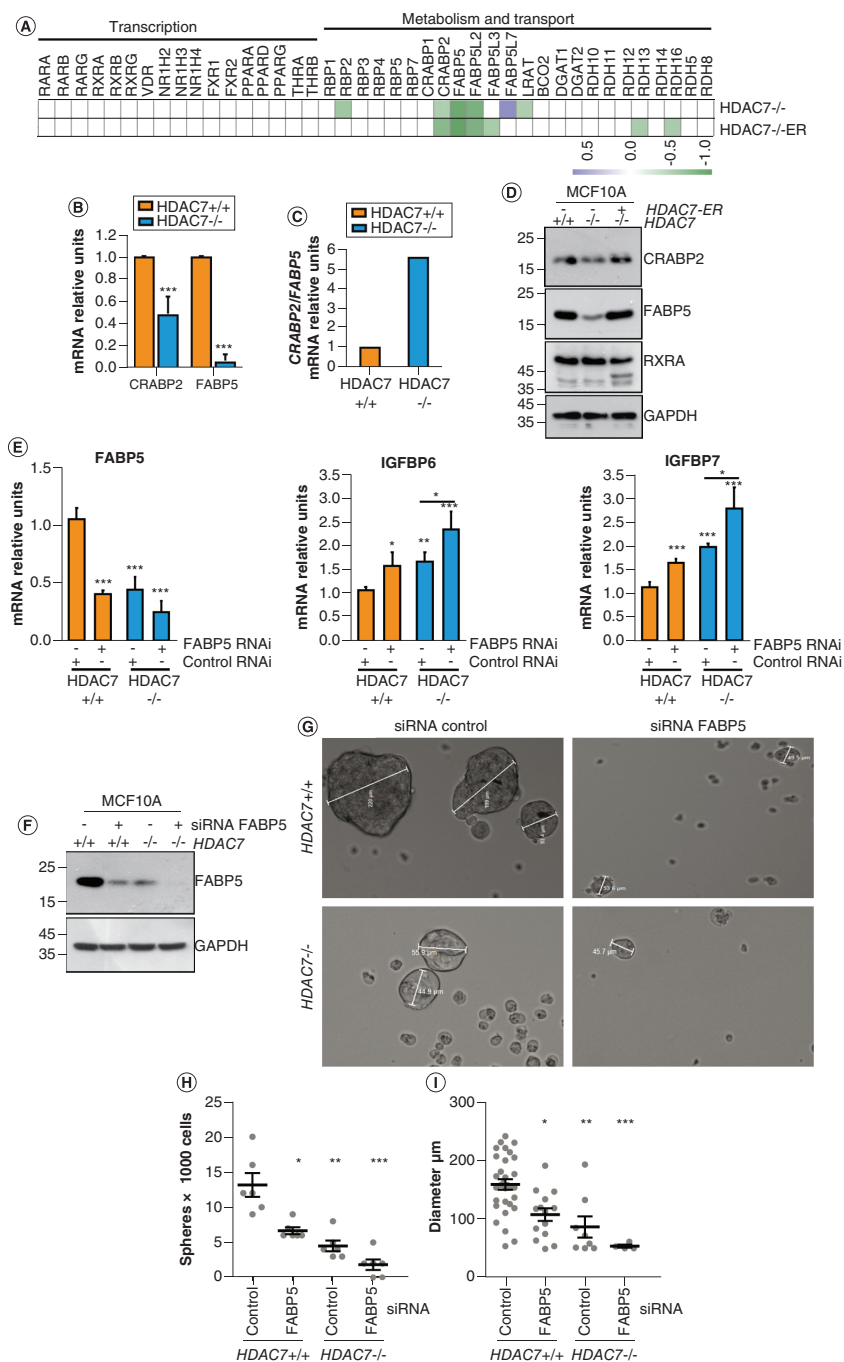
**Figure 4.    HDAC7 can influence expression levels of *CRABP2* and *FABP5*. (A)** Heat map indicating mRNA fold changes between *HDAC7*⁻/⁻ and *HDAC7*⁺/⁺ MCF10A cells and *HDAC7* ⁻/⁻ER and *HDAC7* ⁻/⁻HDAC7-ER MCF10A cells of genes involved in RXRA activity. **(B)** The mRNA expression levels of *CRABP*2 and *FABP5*, as measured by qRT-PCR, in *HDAC7*⁻/⁻ and *HDAC7*⁺/⁺ MCF10A cells. **(C)** The mRNA expression ratio for *CRABP*2 and *FABP5*, as measured by qRT-PCR, in *HDAC7*⁻/⁻ and *HDAC7*⁺/⁺ MCF10A cells. **(D)** Immunoblot analysis of CRABP2 and FABP5 levels in *HDAC7* ⁻/⁻, *HDAC7*⁺/⁺ and *HDAC7*⁻/⁻ MCF10A cells re-expressing HDAC7-ER. Cellular lysates were generated and immunoblots performed with the indicated antibodies. GAPDH was used as loading control. **(E)** *HDAC7*⁻/⁻ and *HDAC7*⁺/⁺ MCF10A cells were grown for 72 h in the presence of the indicated siRNAs. After cell lysis, mRNA expression levels of *FABP5, IGFBP6* and *IGFBP7* were measured by quantitative real-time PCR. **(F)** Immunoblot analysis of FABP5 levels in *HDAC7*⁺/⁺ and *HDAC7*⁻/⁻ MCF10A cells transfected with RNAi against *FABP5* or control RNAi. Cellular lysates were generated and immunoblots performed with the anti-FABP5 antibody. The anti-GAPDH antibody was used as loading control. **(G)** Representative phase contrast images of mammospheres generated by *HDAC7*⁺/⁺ and *HDAC7*⁻/⁻ MCF10A cells transfected with RNAi against *FABP5* or control RNAi after 5 days in culture (n = 3). **(H)** Scatter dot plot illustrating the number of mammospheres generated by *HDAC7*⁺/⁺ and *HDAC7*⁻/⁻ MCF10A cells transfected with RNAi against *FABP5* or control RNAi after 5 days in culture (n = 3). **(I)** Scatter dot plot illustrating the dimension of mammospheres generated by *HDAC7*⁺/⁺ and *HDAC7*⁻/⁻ MCF10A cells transfected with RNAi against *FABP5* or control RNAi after 5 days in culture (n = 3).
*p < 0.05; **p < 0.01; ***p < 0.005.
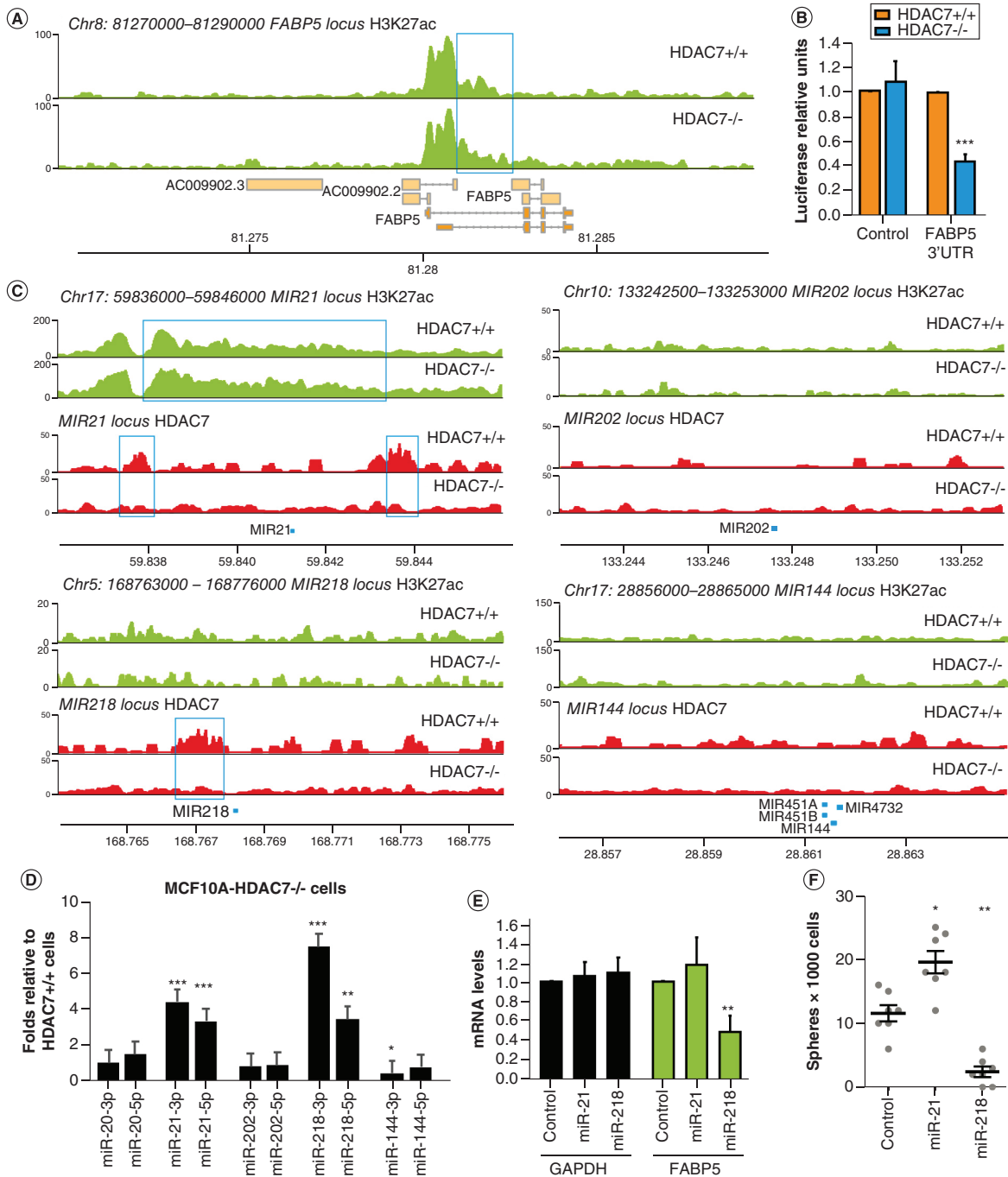
**Figure 5.   Translational regulation of *FABP5* expression. (A)** Detailed view of H3K27ac and HDAC7 tracks at the FABP5 locus in *HDAC7*$^{-/-}$ and *HDAC7*$^{+/+}$ MCF10A cells. Gene structure and chromosomal location are shown, with the blue box highlighting differences in the enriched peaks between the two cell lines. **(B)** Bar graphs showing the results of luciferase assays in *HDAC7*$^{+/+}$ and *HDAC7*$^{-/-}$ MCF10A cells transfected for 48 h with pGL3 control or pGL3 containing the 3′UTR FABP5. *Renilla* sp luciferase was used as internal control (n = 3). **(C)** Detailed view of H3K27ac and HDAC7 tracks at the indicated miRNA loci in *HDAC7*$^{-/-}$ and *HDAC7*$^{+/+}$ MCF10A cells. Gene structure and chromosomal location are shown, with the blue box highlighting differences in the enriched peaks between the two cell lines. **(D)** Expression level rates between *HDAC7*$^{-/-}$ and *HDAC7*$^{+/+}$ MCF10A cells of the indicated miRNAs, as measured by quantitative real-time PCR. **(E)** The mRNA expression levels of *GAPDH* and *FABP5*, as measured by quantitative real-time PCR, in MCF10A cells transfected with miR-21 and miR-218 mimics or scramble control (n = 3). **(F)** Scatter dot plot illustrating the number of mammospheres generated by MCF10A cells transfected with miR-21 and miR-218 mimics or scramble control after 5 days in culture (n = 3).
*p < 0.05; **p < 0.01; ***p < 0.005.

number of spheres, whereas hsa-miR-21 increased their number (Figure 5F). In conclusion, hsa-miR-218 could be involved in the regulation of *FABP5* expression and mammosphere formation in MCF10A cells.

## Discussion

The role of HDAC7 in controlling the stemness of both normal and cancer cells has been reported by different studies [7–9,36,37]. By contrast, the mechanisms and genes that are supervised by HDAC7 for the regulation of stemness features are less defined. It is possible that different signaling pathways under HDAC7 regulation converge in the regulation of stemness properties. The authors have recently shown that a consistent pool of genes repressed by HDAC7 encode for secreted and plasma membrane proteins [9]. In particular, these genes include inflammatory and antiproliferative cytokines and mediators of the immune response. This specific milieu of factors could be particularly critical to sustaining or repressing the growth of stem-like cells [6].

Here the authors provide evidence that elements of IGF signaling can also be repressed by HDAC7. In particular, the authors have found that AKT is less phosphorylated in response to IGF1 when HDAC7 is deleted. The expression of *IGFBP6* and *IGFBP7*, which encode for proteins that can buffer IGF signaling [26,38], is repressed by HDAC7. Therefore, it is plausible that the increase in IGFBP6/7 observed in MCF10A/*HDAC7*$^{-/-}$ cells is responsible for reduced IGF1 activity. To underline the importance of IGF1 signaling in stemness, the authors have demonstrated that recombinant IGF1 increases mammosphere formation in MCF10A cells. In agreement with the authors' observation, a similar result was recently obtained using MCF10A cells expressing constitutively activated IGF1R [39]. In cells knocked out for HDAC7, IGF1 was less efficient in generating mammospheres compared with WT cells. This result confirms that other mechanisms controlling mammosphere formation are under the regulation of HDAC7. These additional mechanisms could involve the regulation of stemness genes through the modulation of superenhancers [10].

HDAC7 does not bind directly to DNA; instead, it assembles into multiprotein complexes, which include DNA-binding TFs. Among them, the family of MEF2 TFs are important partners of HDAC7. However, in MCF10A cells, *IGFPB6* and *IGFPB7* are not direct targets of MEF2s [9]. The control of IGF1 signaling by class IIa HDACs is not a novel concept [40,41]. However, the mechanism involved in this regulation has never been investigated in detail. By using an unbiased motif-based discovery strategy, the authors have found that RXRA and FOXA1 could be involved in the upregulation of *IGFPB6* and *IGFPB7* observed in MCF10A/*HDAC7*$^{-/-}$ cells. RNAi experiments excluded FOXA1 and established that the upregulation of *IGFBP6* and *IGFBP7* observed in MCF10A/*HDAC7*$^{-/-}$ cells was mediated by RXRA. A previous study indicated that RXR isoforms could regulate *IGFBP6* expression in breast cancer cells in response to synthetic rexinoid bexarotene [42]. In addition, the authors' data represent the first report linking RXRA to the control of *IGFBP7* expression. Interestingly, *IGFBP7* could represent a common target of different signaling pathways in sustaining stem cell features. In this respect, the role of IGFBP7 as an inhibitor of the expansion and aggressiveness of tumor stem-like cells was recently demonstrated *in vivo* [27].

The repression exerted by HDAC7 on these IGFBPs seemed to exclude direct binding to RXRA. We suggest that the effect could be indirect and may involve control of *CRABP2* and *FABP5* expression through the action of HDAC7. These genes belong to a family of cellular atRA transporters that shepherd the poorly aqueous soluble retinoids during uptake, metabolism and function [35]. CRABP2 and FABP5 compete for atRA, delivering it to RARs and PPARbeta/delta, respectively [43,44]. HDAC7 is required to sustain higher levels of FABP5, thus favoring PPARbeta/delta transcriptional activities with respect to RXRA. Therefore, in the absence of HDAC7, the delivery of atRA to RXRA should be prevalent. This resetting could be responsible for the upregulation of *IGFBP6* and *IGFBP7* expression.

The dramatic downregulation of *FABP5* expression after HDAC7 deletion did not involve overt H3K27ac modifications at its promoter. Instead, the stability of the 3′UTR FABP5 was compromised in the absence of HDAC7. The miRNAs that targeted *FABP5* and were under the repressive influence of HDAC7 could be responsible for its degradation. A few miRNAs have been characterized for their ability to target *FABP5*. These include hsa-mir-21 and hsa-mir-144 [45,46]. The authors have shown that hsa-mir-21 and, expecially, hsa-mir-218 are upregulated after deletion of HDAC7. However, only hsa-mir-218 is able to repress *FABP5* and mammosphere generation. It is very likely that other miRNAs under the regulation of HDAC7 are involved in the control of *FABP5* expression. Further studies are needed for their identification and characterization.

*FABP5* is an important target of HDAC7 in the regulation of stemness in MCF10A cells. FABP5 can control IGFBP6/7 mRNA levels, thus sustaining the authors' proposed regulatory axis in which HDAC7 affects RXRA

and *IGFBP6/7* transcription by controlling *FABP5* mRNA stability, possibly through hsa-mir-218 and additional miRNAs, to maintain IGF1 signaling and stem cell properties. Clearly, further experiments are necessary to understand how HDAC7 can exert a repressive action against hsa-mir-218 expression.
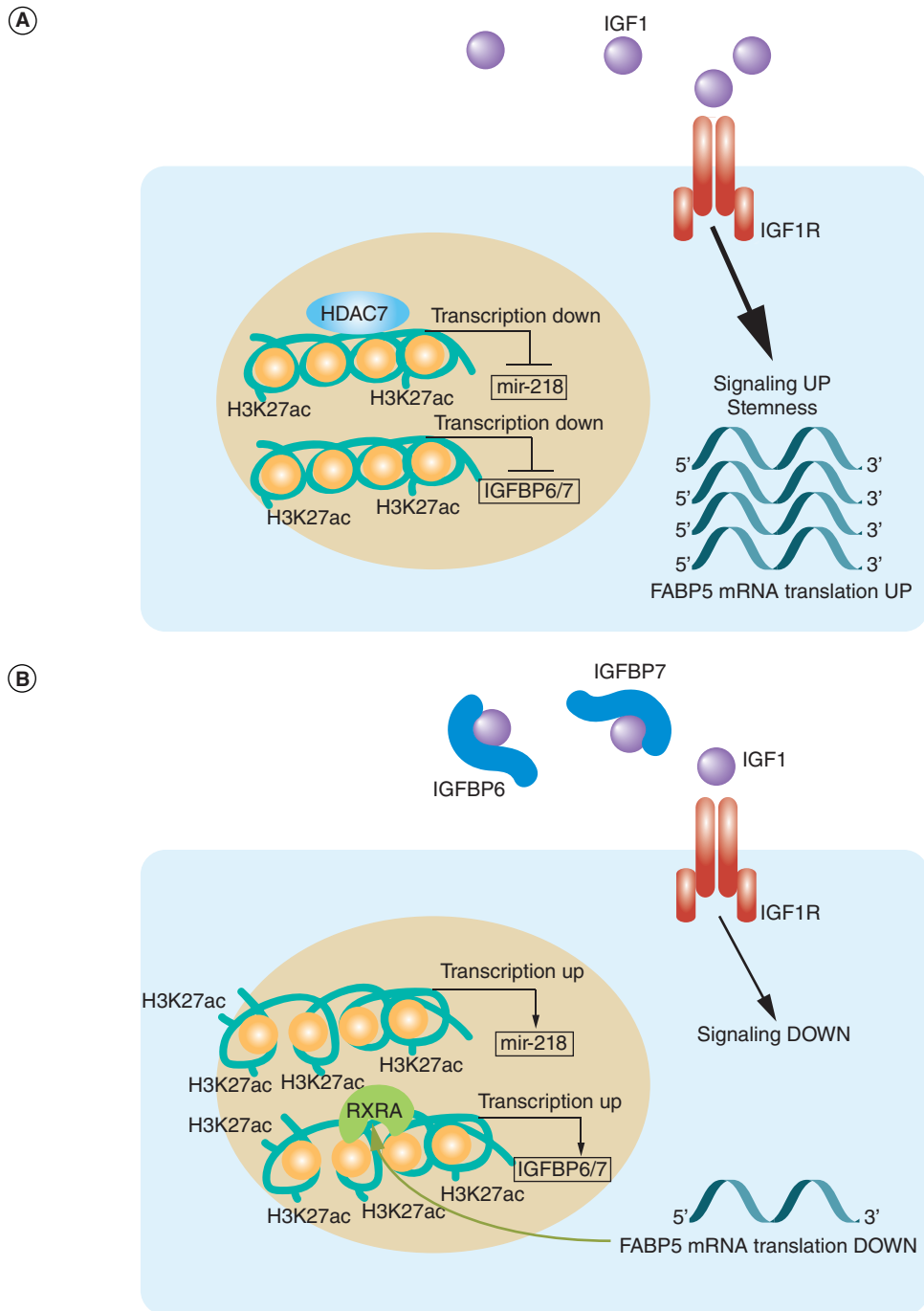


**Figure 6.   The regulative circuit linking HDAC7 to *IGFBP6* and *IGFBP7* expression. (A)** In the presence of HDAC7 mir-218 expression is silences, FABP5 is expressed at high level and IGFBP6/7 levels reduced. **(B)** Removal of HDAC7 unregulated mir-218 expression in absence of overt variations in H327ac levels. FABP5 mRNA levels decrease with the up regulation, RXRA-mediated, of IGFBP6/7 and down regulation of IGF1 signaling.

## Conclusion

We have investigated a new regulative circuit supervised by HDAC7 that can repress the transcription of *IGFBP6* and *IGFBP7*. This circuit can promote IGF1 signaling and stemness properties. A representative schema of the circuit is shown in Figure 6. Our results sustain the view of HDAC7 and class IIa HDACs in general as pleiotropic epigenetic regulators that influence the expression of several genes in a context-dependent manner.

## Future perspective

Studies on the contribution of HDAC7 to the regulation of stemness properties are still in their infancy. Our results add a new piece to the complex puzzle represented by the regulative circuits supervised by HDAC7 in the control of gene expression. There are still several open questions that deserve further investigation. For example, it is unclear through which partners, in addition to MEF2 TFs, HDAC7 acts to control gene expression. Similarly, the subunits of the super-repressive complex engaged by HDAC7 to control stemness must be identified as well as the post-transcriptional modifications that control HDAC7 activity.

### Summary points

- HDAC7 controls H3K27ac levels in the regulative regions and expression of *IRS2*, *IGFBP6* and *IGFBP7*.
- IGF1 sustains mammosphere formation.
- In the absence of HDAC7, RXRA promotes *IGFBP6* and *IGFBP7* expression.
- HDAC7 counteracts RXRA activity indirectly by allowing high levels of *FABP5* mRNA and protein.
- The action of HDAC7 on *FABP5* mRNA levels is indirect and could be mediated by hsa-mir-218.

## References

Papers of special note have been highlighted as: ● of interest; ●● of considerable interest

1.  Parra M. Class IIa HDACs – new insights into their functions in physiology and pathology. *FEBS J.* 282(9), 1736–1744 (2015).

2.  Di Giorgio E, Brancolini C. Regulation of class IIa HDAC activities: it is not only matter of subcellular localization. *Epigenomics.* 8(2), 251–269 (2015).

3.  Clocchiatti A, Di Giorgio E, Ingrao S, Meyer-Almes F-J, Tripodo C, Brancolini C. Class IIa HDACs repressive activities on MEF2-depedent transcription are associated with poor prognosis of ER+ breast tumors. *FASEB J.* 27, 942–954 (2013).

4.  Clocchiatti A, Di Giorgio E, Viviani G *et al.* The MEF2–HDAC axis controls proliferation of mammary epithelial cells and acini formation *in vitro*. *J. Cell Sci.* 128(21), 3961–3976 (2015).

● **Definition of the role of HDAC7 in the morphogenetic process that leads to acini formation *in vitro*.**

5.  Marks DL, Olson RL, Fernandez-Zapico ME. Epigenetic control of the tumor microenvironment. *Epigenomics* 8(12), 1671–1687 (2016).

6.  Hageman JH, Heinz MC, Kretzschmar K, van der Vaart J, Clevers H, Snippert HJG. Intestinal regeneration: regulation by the microenvironment. *Dev. Cell* 54(4), 435–446 (2020).

7.  Broholm C, Ribel-Madsen R, Hjort L *et al.* Epigenome- and transcriptome-wide changes in muscle stem cells from low birth weight men. *Endocr. Res.* 45(1), 58–71 (2020).

8.  Witt AE, Lee CW, Lee TI *et al.* Identification of a cancer stem cell-specific function for the histone deacetylases, HDAC1 and HDAC7, in breast and ovarian cancer. *Oncogene* 36(12), 1707–1720 (2017).

•• Unveils the role of HDAC7 in breast cancer and ovarian stem cell regulation.

9.  Cutano V, Di Giorgio E, Minisini M, Picco R, Dalla E, Brancolini C. HDAC7-mediated control of tumour microenvironment maintains proliferative and stemness competence of human mammary epithelial cells. *Mol. Oncol.* 13(8), 1651–1668 (2019).

•• Definition of the role of HDAC7 in the control of IL-24 expression and mammosphere formation.

10. Caslini C, Hong S, Ban YJ, Chen XS, Ince TA. HDAC7 regulates histone 3 lysine 27 acetylation and transcriptional activity at super-enhancer-associated genes in breast cancer stem cells. *Oncogene* 38(39), 6599–6614 (2019).

11. Liu B, Chen F, Wu Y *et al.* Enhanced tumor growth inhibition by mesenchymal stem cells derived from iPSCs with targeted integration of interleukin24 into rDNA loci. *Oncotarget* 8(25), 40791–40803 (2017).

12. Kleinberg DL, Barcellos-Hoff MH. The pivotal role of insulin-like growth factor I in normal mammary development. *Endocrinol. Metab. Clin. North Am.* 40(3), 461–471 (2011).

13. Christopoulos PF, Msaouel P, Koutsilieris M. The role of the insulin-like growth factor-1 system in breast cancer. *Mol. Cancer* 14, 43 (2015).

14. Chang Wen-Wei, Lin Ruey-Jen, John Yu *et al.* The expression and significance of insulin-like growth factor-1 receptor and its pathway on breast cancer stem/progenitors. *Breast Cancer Res.* 15(3), R39 (2013).

15. Tominaga K, Shimamura T, Kimura N *et al.* Addiction to the IGF2-ID1-IGF2 circuit for maintenance of the breast cancer stem-like cells. *Oncogene* 36(9), 1276–1286 (2017).

16. Paluvai H, Di Giorgio E, Brancolini C. Unscheduled HDAC4 repressive activity in human fibroblasts triggers TP53-dependent senescence and favors cell transformation. *Mol. Oncol.* 12(12), 2165–2181 (2018).

17. Di Giorgio E, Gagliostro E, Clocchiatti A, Brancolini C. The control operated by the cell cycle machinery on MEF2 stability contributes to the downregulation of CDKN1A and entry into S phase. *Mol. Cell Biol.* 35(9), 1633–1647 (2015).

18. Paroni G, Mizzau M, Henderson C, Del Sal G, Schneider C, Brancolini C. Caspase-dependent regulation of histone deacetylase 4 nuclear-cytoplasmic shuttling promotes apoptosis. *Mol. Biol. Cell* 15(6), 2804–2818 (2004).

19. Di Giorgio E, Clocchiatti A, Piccinin S *et al.* MEF2 is a converging hub for histone deacetylase 4 and phosphatidylinositol 3-kinase/Akt-induced transformation. *Mol. Cell Biol.* 33(22), 4473–4491 (2013).

20. Ritchie ME, Phipson B, Wu D *et al.* limma powers differential expression analyses for RNA-sequencing and microarray studies. *Nucleic Acids Res.* 43(7), e47 (2015).

21. Langmead B, Salzberg SL. Fast gapped-readalignment with Bowtie. *Nat. Methods* 9(4), 357–359 (2012).

22. Heinz S, Benner C, Spann N *et al.* Simple combinations of lineage-determining transcription factors prime cis-regulatory elements required for macrophage and B cell identities. *Mol. Cell* 38(4), 576–589 (2010).

23. Yu G, Wang L, He Q. Genome analysis ChIPseeker: an R / Bioconductor package for ChIP peak annotation, comparison and visualization. *Bioinformatics* 31(14), 2382–2383 (2015).

24. Hahne F, Ivanek R. Visualizing genomic data using Gviz and Bioconductor. *Methods Mol. Biol.* 1418, 335–351 (2016).

25. Chen C, Ridzon DA, Broomer AJ *et al.* Real-time quantification of microRNAs by stem-loop RT-PCR. *Nucleic Acids Res.* 33(20), e179 (2005).

26. Bach LA, Hale LJ. Insulin-like growth factors and kidney disease. *Am. J. Kidney Dis.* 65(2), 327–336 (2015).

27. Cao Z, Scandura JM, Inghirami GG, Shido K, Ding BS, Rafii S. Molecular checkpoint decisions made by subverted vascular niche transform indolent tumor cells into chemoresistant cancer stem cells. *Cancer Cell* 31(1), 110–126 (2107).

•• Demonstrates that IGFBP7 blocks IGF1 and inhibits expansion and aggressiveness of tumor stem-like cells.

28. Di Giorgio E, Hancock WW, Brancolini C. MEF2 and the tumorigenic process, hic sunt leones. *Biochim. Biophys. Acta Rev. Cancer* 1870(2), 261–273 (2018).

29. Lee C, Huang CH. LASAGNA-Search: an integrated web tool for transcription factor binding site search and visualization. *Biotechniques* 54(3), 141–153 (2013).

30. Machanick P, Bailey TL. MEME-ChIP: motif analysis of large DNA datasets. *Bioinformatics* 27(12), 1696–1697 (2011).

31. Yevshin I, Sharipov R, Valeev T, Kel A, Kolpakov F. GTRD: a database of transcription factor binding sites identified by ChIP-seq experiments. *Nucleic Acids Res.* 45(D1), D61–D67 (2017).

32. Wang Y, Song F, Zhang B *et al.* The 3D Genome Browser: a web-based browser for visualizing 3D genome organization and long-range chromatin interactions. *Genome Biol.* 19(1), 151 (2018).

33. Di Giorgio E, Franforte E, Cefalù S *et al.* The co-existence of transcriptional activator and transcriptional repressor MEF2 complexes influences tumor aggressiveness. *PLoS Genet.* 13(4), e1006752 (2017).

34. Garattini E, Bolis M, Garattini SK *et al.* Retinoids and breast cancer: from basic studies to the clinic and back again. *Cancer Treat. Rev.* 40(6), 739–749 (2014).

35. Napoli JL. Cellular retinoid binding-proteins, CRBP, CRABP, FABP5: effects on retinoid metabolism, function and related diseases. *Pharmacol. Ther.* 173, 19–33 (2017).

36. Compagnucci C, Barresi S, Petrini S, Bertini E, Zanni G. Rho-kinase signaling controls nucleocytoplasmic shuttling of class IIa histone deacetylase (HDAC7) and transcriptional activation of orphan nuclear receptor NR4A1. *Biochem. Biophys. Res. Commun.* 459(2), 179–183 (2015).

37. Bang SY, Kwon SH, Yi SH *et al.* Epigenetic activation of the Foxa2 gene is required for maintaining the potential of neural precursor cells to differentiate into dopaminergic neurons after expansion. *Stem Cells Dev.* 24(4), 520–533 (2015).

38. Evdokimova V, Tognon CE, Benatar T *et al.* IGFBP7 binds to the IGF1 receptor and blocks its activation by insulin-like growth factors. *Sci. Signal.* 5(255), ra92 (2012).

39. Farabaugh SM, Litzenburger BC, Elangovan A *et al.* IGF1R constitutive activation expands luminal progenitors and influences lineage differentiation during breast tumorigenesis. *Dev. Biol.* 463(1), 77–87 (2020).

40. Peruzzo P, Comelli M, Di Giorgio E, Franforte E, Mavelli I, Brancolini C. Transformation by different oncogenes relies on specific metabolic adaptations. *Cell Cycle* 15(19), 2656–2668 (2016).

41. Malinen M, Ryynänen J, Heinäniemi M, Väisänen S, Carlberg C. Cyclical regulation of the insulin-like growth factor binding protein 3 gene in response to 1alpha,25-dihydroxyvitamin D3. *Nucleic Acids Res.* 39(2), 502–12 (2011).

42. Uray IP, Shen Q, Seo HS *et al.* Rexinoid-induced expression of IGFBP-6 requires RARbeta-dependent permissive cooperation of retinoid receptors and AP-1. *J. Biol. Chem.* 284(1), 345–353 (2009).

43. Schug TT, Berry DC, Shaw NS, Travis SN, Noy N. Opposing effects of retinoic acid on cell growth result from alternate activation of two different nuclear receptors. *Cell* 129(4), 723–733 (2007).

•• **Provides evidence that partitioning of retinoic acid between the two receptors is regulated by CRABP-II and FABP5.**

44. Schug TT, Berry DC, Toshkov IA, Cheng L, Nikitin AY, Noy N. Overcoming retinoic acid resistance of mammary carcinomas by diverting retinoic acid from PPARbeta/delta to RAR. *Proc. Natl Acad. Sci. U. S. A.* 105(21), 7546–7551 (2008).

45. Ni K, Wang D, Xu H *et al.* miR-21 promotes non-small cell lung cancer cells growth by regulating fatty acid metabolism. *Cancer Cell Int.* 19, 219 (2019).

46. Zhang C, Liao Y, Liu P *et al.* FABP5 promotes lymph node metastasis in cervical cancer by reprogramming fatty acid metabolism. *Theranostics* 10(15), 6561–6580 (2020).